Surface Plasmon Resonance Phase-Sensitive Imaging (SPR-PI) Sensor Based on a Novel Prism Phase Modulator

Gaoao Ye, Wei Yang, Li Jiang, and Sailing He[*]

Abstract—A novel prism phase modulator (PPM) for phase difference modulation between *p*- and *s*-polarization lights in a surface plasmon resonance phase-sensitive imaging sensor is proposed in this paper. The PPM consists of a rhombic prism (to obtain a curve of phase difference between the two polarizations), a rotation stage and a mirror. The PPM shows great modulation stability and helps to achieve a high detection resolution. Surface plasmon resonance phase imaging is realized with a microfluidic device and a CCD camera. Experimental result shows that the detection resolution of our SPR-PI sensor based on phase-interrogation method is 7.61×10^{-7} RIU with hydrous samples, which is 16 times improved compared with that based on intensity-interrogation. Real-time monitoring of the interaction between Angiogenin and anti-Angiogenin is also illustrated.

1. INTRODUCTION

Surface plasmons are collective electron oscillations at the interface of two materials with negative and positive real parts of dielectrics constant. Optical excitation of surface plasmons occurs when the wave vector of the excitation light matches the propagation constant of the surface plasmons [1]. Due to the dependence of the resonance condition on the refractive index of the material contacting the metal, surface plasmon resonance (SPR) based techniques have been widely applied into biological and chemical detection [1, 2]. Integrated with microfluidic, high-throughput SPR sensors have been realized for various applications [3, 4].

Traditional SPR sensors are based on amplitude-sensitive methods, which consist of intensity, angle and spectral interrogation [5]. These SPR sensors are able to detect the binding events of large molecules (DNA-DNA, antigen-antibody, etc.). However, the performance of the amplitude-sensitive SPR sensors rely heavily on the intensity noise and suffers a detection limit of 10^{-6} RIU [6], which is not enough to detects mall molecules (e.g., drugs). Since the dependence of the phase responseon refractive index is much stronger than that of the amplitude response, phase-sensitive SPR sensor emerges as a promising resolution to provide lower detection limit in late 1990s [7–9]. During the last two decades, phase-sensitive SPR sensors received extensive research in order to improve the detection limit [10], dynamic range [11–14] and detection throughput [15–19].

The phase property of the reflected light in a phase-sensitive SPR sensor can be extracted by optical heterodyne, polarimetry or interferometry [20]. In recent years, phase-sensitive SPR sensors based on polarimetry have been widely exploited for their suitability for 2-dimension detection. To enhance the detection resolution, several kinds of phase modulators were developed to modulate the polarization statue and the phase retardation of the incident light. In 2004, Hooper and Samble employed a faraday rotator [21] and several months later a liquid crystal polarizer [22] to modulate the polarization of the incident light. Wu et al. used a piezoelectric stage to modulate the phase retardation of *p*- and

s-polarization light in a SPR sensor based on Mach-Zehnder configuration [23]. Several years later they applied the piezoelectric stage in a SPR-PI system and obtained a resolution of 8.8×10^{-7} RIU with different glycerine solutions [18]. In 2005, Su and Chen applied a liquid crystal modulator to induce a phase difference between p- and s-polarization of the light in a SPR-PI sensor [24]. They tested their sensor with nitrogen and argon gases and estimate a detection limit of 2×10^{-7} RIU with gaseous samples. In 2006, Ho et al. developed a phase-sensitive SPR sensor using a photoelastic modulator [25]. In 2008, a birefringent wedge was applied to spatially modulate the incident light in a SPR-PI system. By analyzing the interference pattern of different glycerin solutions, Patskovsky and coworkers estimated a resolution of 1×10^{-5} RIU [26].

In this paper, we propose a novel prism phase modulator (PPM) in a SPR phase-sensitive imaging (SPR-PI) sensor based on polarimetry. We utilize total internal reflection (TIR) to temporally modulate the phase difference between p- and s-polarization light. Compared with conventional modulators, the main advantage of the PPM is its TIR-based modulation which does not need electrical signal to control the phase stepping. The modulation of the PPM is based on the scanning of the incident angle and can be easily realized with a motor rotation stage. Since the refractive index of the glass is insensitive to temperature, the TIR-based modulation shows excellent thermal stability. The PPM holds several other advantages as low-cost, easy to use and etc.. Combined with a microfluidic chip and a scientific grade CCD, 2-dimension detection of samples in different channels of the microfluidic chip is realized.

2. THEORETICAL ANALYSIS

2.1. SPR Excitation

The propagation constant of the surface plasmons confined to the interface of a semi-infinite dielectric and a semi-infinite metal can be expressed as

$$\beta_{sp} = \frac{w}{c}\sqrt{\frac{\varepsilon_d \varepsilon_m}{\varepsilon_d + \varepsilon_m}} \tag{1}$$

where w is the angular frequency of the excitation light and c the speed of light in vacuum. ε_d and ε_m are the dielectric constants of the dielectric and the metal, respectively. Since ε_m is a complex number, β_{sp} can be further written as

$$\beta_{sp} = \frac{w}{c}(n_{ef} + i\gamma_i) \tag{2}$$

n_{ef} and γ_i are the effective refractive index and the attenuation coefficient of the surface plasmon, respectively. The Kretschmann configuration is the most widely used method for optical excitation of SPR [27]. In the Kretschmann configuration, a $50\,\text{nm}$ gold layer is deposited on the bevel of a coupling prism. An evanescent wave is induced when the incident light is total reflected on the prism-gold interface. The wave vector of the evanescent wave parallel to the interface can be expressed as

$$k_{ev} = \frac{w}{c}n_p \sin\theta \tag{3}$$

where n_p is the refractive index of the coupling prism and θ the incident angle on the prism-gold interface. SPR condition is fulfilled when

$$n_{ef} = n_p \sin\theta \tag{4}$$

Once the surface plasmon is resonantly excited, the reflected p-polarization light undergoes dramatic intensity attenuation and phase jump, while those characteristics of s polarization light remain unchanged. As a result, a phase difference between p and s polarization light φ_{spr} is created after SPR. When the incident angle is fixed, the value of φ_{spr} is mainly determined by the refractive index of the sample contacting the metal.

2.2. Modulation Principle of PPM

In our proposed PPM, total internal reflection (TIR) in an uncoated rhombic prism is applied to modulate the phase difference between p- and s-polarization light. It is well known that TIR occurs on

a glass/air interface when the incident angle θ_i is greater than the critical angle. The reflectivity of p- and s-polarization light can be predicted using the Fresnel formula,

$$r_p = \frac{\cos\theta_i - n\sqrt{1 - (n\sin\theta_i)^2}}{\cos\theta_i + n\sqrt{1 - (n\sin\theta_i)^2}} = |r_p|\,e^{i\varphi_p} \tag{5}$$

$$r_s = \frac{n\cos\theta_i - \sqrt{1 - (n\sin\theta_i)^2}}{n\cos\theta_i + \sqrt{1 - (n\sin\theta_i)^2}} = |r_s|\,e^{i\varphi_s} \tag{6}$$

n represents the refractive index of the glass. $|r_p|$ and $|r_s|$ are defined as the absolute values of the reflectivity of the p-polarization light and s-polarization light, respectively. φ_p and φ_s are the phase shifts of p- and s-polarization lights after the TIR, respectively. In the TIR condition, $|r_p| = |r_s| = 1$. φ_p and φ_s can be extracted from Eq. (5) and Eq. (6), respectively.

$$\varphi_p = -2\tan^{-1}\frac{n\sqrt{n^2\sin^2\theta_i - 1}}{\cos\theta_i} \tag{7}$$

$$\varphi_s = -2\tan^{-1}\frac{\sqrt{n^2\sin^2\theta_i - 1}}{n\cos\theta_i} \tag{8}$$

The phase difference $\Delta\varphi$ after one time TIR can be calculated as follow,

$$\Delta\varphi = \varphi_p - \varphi_s = 2\tan^{-1}\left(\frac{\cos\theta_i\sqrt{n^2\sin^2\theta_i - 1}}{n\sin^2\theta_i}\right) \tag{9}$$

$\Delta\varphi$ is determined by the refractive index of the glass and the incident angle. By scanning the incident angle, we can continuously modulate the phase difference between p- and s-light beams, while keeping their magnitudes unchanged. This unique characteristic of the TIR makes it quite suitable to be used as a phase difference modulator in polarimetric phase-sensitive SPR sensors. Fig. 1(a) shows the simulation result of the phase shifts of p- and s-polarization light at different incident angles. As we can see, the phase shift of p-polarization light increases faster than that of s-polarization light when the incident angle increases from 40 degree to 50 degree. The difference of the phase shifts between the p- and s-polarization light reaches a maximum (0.8 rad) at 50 degree and then gradually decreases to zero at 90 degree. By scanning the incident angle from 40 degree to 50 degree, the phase difference can be modulated from 0 to 0.8 rad (indicated as the orange region).
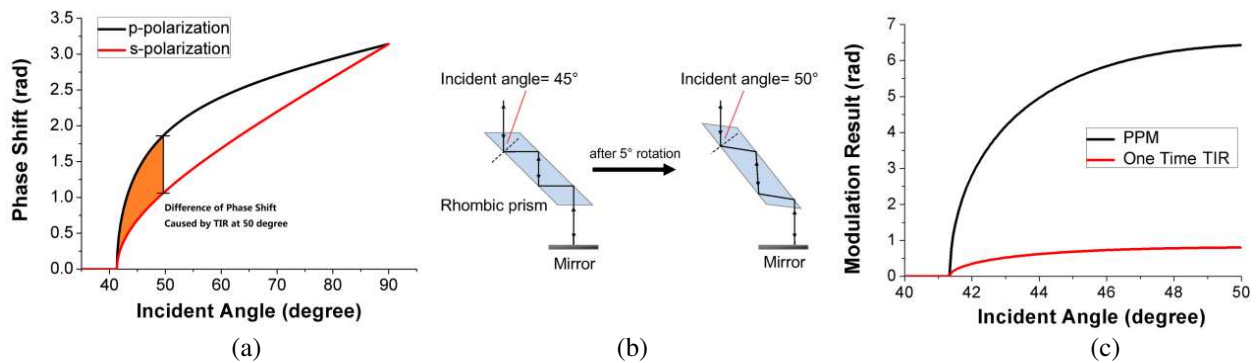
Figure 1. (a) Curves of the simulated phase shifts of p- and s-polarization light for one time total internal reflection. The glass refractive index is set to be 1.515 in the simulation. (b) The arrangement of PPM (the rotation stage is not shown) and the detailed light-path in therhombic prism when the incident angle is 45 degree (left) and 50 degree (right), respectively. (c) The modulation result for one time TIR and the PPM (8 times TIR).

The main challenge involved in the application of the TIR modulation is to keep the output light-path during the scanning of the incident angle. In the design of the PPM, a rotational rhombic prism and a mirror are combined to solve the problem. Fig. 1(b) shows the arrangement of our PPM and the detailed light-path when the incident angle is 45° and 50°. In each of these two conditions, the light beam incidents normally onto the mirror with a horizontal displacement. After reflected from the mirror, the light beam goes back into the rhombic prism and the horizontal displacement is compensated. As a result, the light-path of the output light beam is kept during modulation. The total modulated phase difference (8 times TIR) can be obtained by subtracting the phase shift of p-polarization light with that of s-polarization light,

$$\varphi_m = 8\Delta\varphi = 16\tan^{-1}\left(\frac{\cos\theta_i\sqrt{n^2\sin^2\theta_i - 1}}{n\sin^2\theta_i}\right) \tag{10}$$

Fig. 1(c) shows the simulated modulation result for one time TIR and the PPM when the incident angle scans from 40° to 50°. The modulation depth of the PPM with 8 times TIR is about 2π. Greater modulation depths can be achieved by increasing the length of the rhombic prism, or assembling two or more rhombic prisms together.

3. EXPERIMENT

3.1. Materials

3,3'-Dithiodi propionic acid (DDA), N-(3-Dimethylaminopropyl)-N'-ethylcarbodiimide hydrochloride (EDC), and N-Hydroxysuccinimide (NHS), were purchased from Sigma-Aldrich. Phosphate-buffered saline (PBS) at PH 7.4 and deionized water (DI water) were homemade. Angiogenin and anti-Angiogenin were obtained from a collaborator's lab.

3.2. System Setup

The schematic of our SPR phase-sensitive imaging sensor is shown in Fig. 2. A stabilized laser (671 nm) is used as the light source. After linearly polarized, the light goes through the beam splitter and incidents into a BK7 rhombic prism (length/height ratio 4 : 1). The rhombic prism is fixed on a motor-driven rotation stage. A lab-built LabVIEW program (National Instruments, Austin, TX, USA) is developed to manipulate the rotation angle and speed. The modulated light is then focused by an objective and filtered with a pin hole. After reflected from the SPR sensor, the light beam incidents into the imaging system including an imaging lens, an analyzer and a CCD. To achieve high image quality over the whole SPR sensing surface, we tilted the CCD to match with the image plane. Clear pictures were obtained over a large area as shown in the right-bottom inset of Fig. 2.
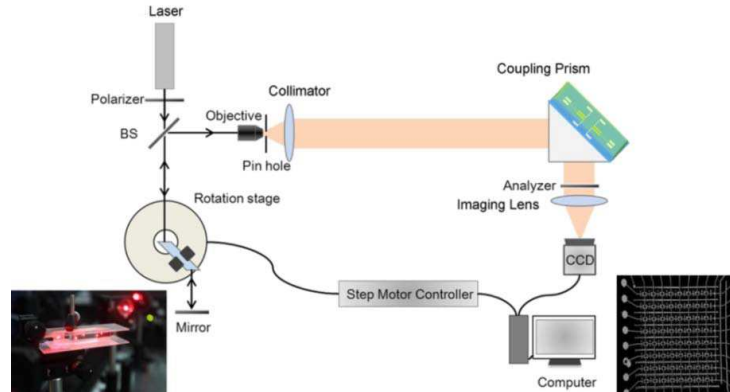
Figure 2. Schematic diagram the setup of our PPM-based SPR sensor. BS stands for beam splitter. The left-bottom inset is the photograph of the PPM. The right-bottom inset shows the SPR image of a homemade microfluidic channels captured by the CCD.

3.3. Data Processing

The interference intensity between the projections of p and s light can be written as

$$I = I_p + I_s + 2\sqrt{I_p I_s}\cos(\varphi_m + \varphi_{spr}) \tag{11}$$

I_p and I_s are the projection intensities of p- and s-light on the axis of the linear analyzer, respectively. A series of interference intensities can be obtained after a round of full-range modulation, which takes 14 modulation steps and costs about 14 seconds. Fig. 3(a) illustrates the details of the rotation stage angle, TIR incident angle and modulation result of the PPM during the 14-step modulation. The rotation stage angle is defined as 0 degree when the TIR incident angle is 45 degree. A MATLAB program (MathWorks, Natick, MA, USA) is applied to process the captured pictures. Typically, the region of interest in the picture is manually selected. The grey scales of pixels in the selected region are averaged and saved as the interference intensities. Combined with the modulation steps of the PPM, a dependence curve of the interference intensity on the modulation result of the PPM can be obtained. Fig. 3(b) shows a typical series of interference intensities during the 14-step modulation and the fitted cosine curve. The coefficient 0.7565 of the fitted curve equation represents the value of φ_{spr} extracted in one full-range modulation.

Modulation Step	1	2	3	4	5	6	7	8	9	10	11	12	13	14
Rotation Stage Angle (degree)	5.47	5.38	5.27	5.12	4.96	4.73	4.46	4.18	3.79	3.43	2.57	1.84	1.06	0.47
TIR Incident Angle (degree)	41.39	41.45	41.52	41.62	41.72	41.88	42.05	42.24	42.50	42.74	43.30	43.78	44.30	44.69
Modulation Result (rad)	0.80	1.16	1.50	1.87	2.18	2.55	2.91	3.22	3.60	3.89	4.45	4.82	5.14	5.34

(a)
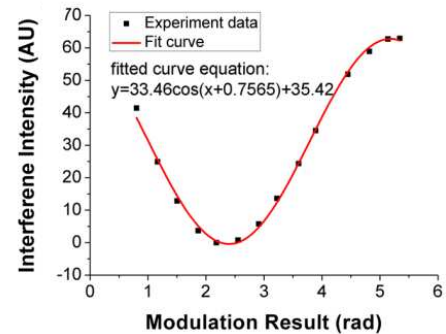
(b)

Figure 3. (a) The rotation stage angle, TIR incident angle and modulation result of the PPM during a 14-setp modulation. (b) Interference intensities and the fitted curve during a 14-step PPM modulation.

To minimize the detection noise, another region of interest is usually selected as a reference region. The phase (intensity) responses of the probe region and the reference region can be calculated separately, thus we can get the SPR phase (intensity) signal by subtracting the response of the probe region with that of the reference region. Undesirable background noises due to the thermal drift, laser intensity fluctuation and mechanical vibration can be remarkably reduced after the subtraction.

In the traditional amplitude-sensitive SPR sensors, the intensity information of I_p is used to determine the refractive index change. In our phase extraction algorithm, the values of $I_p + I_s$ and $\sqrt{I_p I_s}$ are also obtained after curve fitting (as shown in Fig. 3(b)). To distinguish I_p from I_s, the polarizer is adjusted to make I_p slightly stronger than I_s. During continuous modulation, the curves of I_p and I_s can be clearly separated with their beginning values.

4. RESULT AND DISCUSSION

4.1. Modulation Stability

To detect the modulation stability of the PPM, an analyzer and a photo detector were applied before the objective to detect the interference intensity. The interference intensities were recorded during repeated rounds of full-range modulations. The phase information of each full-range modulation was extracted by a curve fitting algorithm. As illustrated in Fig. 4, the extracted phase varies during the 140 round modulations, which takes about 35 min. The modulation stability can be expressed as the standard
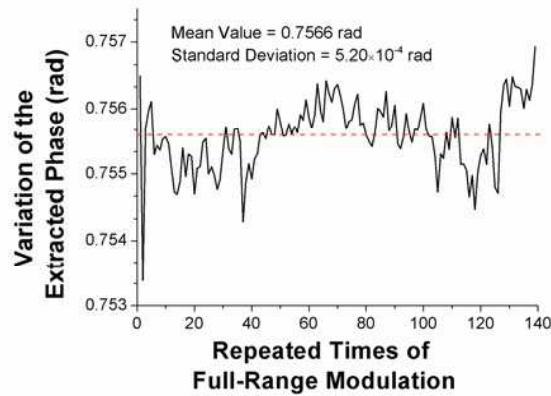
**Figure 4.** Variation of SPR phase signal during long-time continuous modulation.

deviation of the extracted phase,

$$\sigma_m = 5.20 \times 10^{-4}\,\text{rad} = 0.0298\,\text{degree}$$

The modulation stability can be further improved by using an intensity reference of the laser and a rotation stage with a better repeatability.

## 4.2. Detection Resolution Based on Phase Interrogation

The detection resolution test was carried out in a homemade microfluidic chip. The chip consists of 8 horizontal channels and 8 vertical channels. Each channel is linked with an input opening and an output opening. The 8×8 gold sensing areas ($0.5 \times 0.8\,\text{mm}^2$) are located at the crosses of the horizontal and vertical channels (the highlighted square regions in Fig. 5(a)). The channels are separated by micro-valves actuated with high pressure ($\sim 0.15\,\text{MPa}$).

(a)   (b)
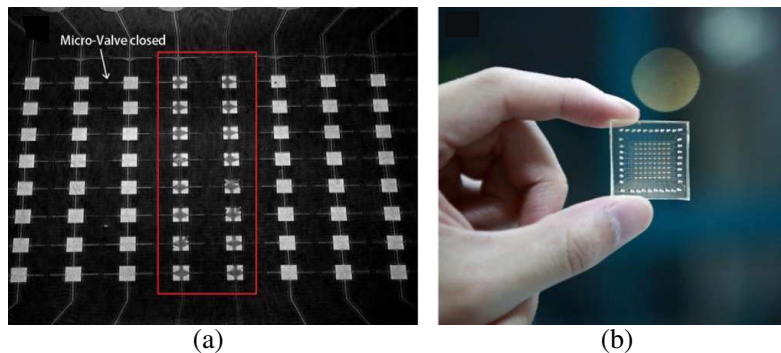
Figure 5. (a) Captured CCD image of the microfluidic device. The vertical micro-valves are closed to allow sample flows vertically. The diamond-shaped dark areas in the gold spots are regions where SPR occur. (b) Photograph of the microfluidic chip.

In the resolution test, two vertical channels were chosen as reference channel and probe channel, as shown in Fig. 5(a). The reference channel was filled with DI water and the probe channel was injected with glycerine solutions with gradient concentration from 0% to 2% one by one. The incident angle on the gold surface was adjusted to meet the best SPR for water. SPR phase signal was extracted with the method described previously.

8 pairs of probe and reference regions at different rows were selected. The detection for one concentration solution was repeated for 15 times and the SPR phase signal was calculated for each
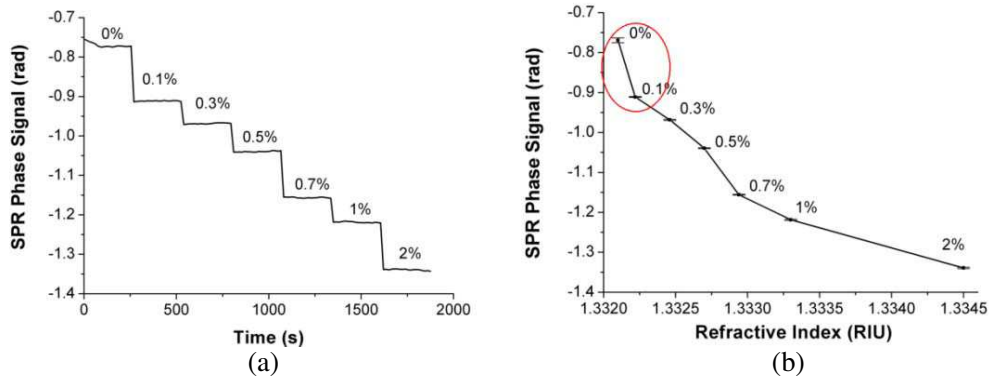
Figure 6. (a) Real time recorded SPR signal when the probe channel is injected with different glycerine solutions. (b) The mean values and the standard deviations of the SPR phase signal with different refractive index solutions.

time. Fig. 6(a) shows the real time SPR phase signal of the third-row probe and reference regions. As we can see, The SPR phase signal decreases gradually when we change the solution from water to 2% glycerine solution.The standard deviations of the glycerine solutions from 0.1% to 2% are 0.0009 rad, 0.0013 rad, 0.0013 rad, 0.0012 rad, 0.0015 rad and 0.0017 rad, respectively. Fig. 6(b) presents the mean values and the standard deviations of SPR phase signals of each concentration. Since the SPR angle was adjusted for water, the SPR phase signal decreases most sharply from water to 0.1% glycerine solution (as indicated in Fig. 6(b)) and gradually becomes less sensitive when the concentration increases.

The region when the glycerine concentration increases from 0% to 0.1% is selected to calculate the phase sensitivity. The sensitivity can be calculated as

$$S_p = \frac{\Delta\varphi_{spr}}{\Delta n} = 1183 \times 10^3 \, \text{rad/RIU}$$

where $\Delta\varphi_{spr}$ and Δn are the change of the SPR phase signal and refractive index, respectively. The standard deviation of 0.1% glycerine solution is regarded as the sensing uncertainty,

$$\sigma_p = 0.0009 \, \text{rad}$$

The detection resolution based on phase interrogation can be calculated as

$$R_p = \frac{\sigma_p}{S_p} = 7.61 \times 10^{-7} \, \text{RIU}$$

4.3. Detection Resolution based on Intensity Interrogation

The information of the SPR intensity signal was also extracted as well as the phase signal after the fitting algorithm. For each solution, 15 repeated SPR intensity signals were obtained after 15 round modulations. Fig. 7(a) represents the variation of the SPR intensity signal when the probe channel was injected with glycerine solutions with different concentrations. When the concentration increases from 0% to 0.1%, the mean value of the SPR intensity signal increases from 10.7468 to 12.3427 (AU). Combined with the change of the refractive index, the sensitivity of the intensity interrogation methods can be calculated,
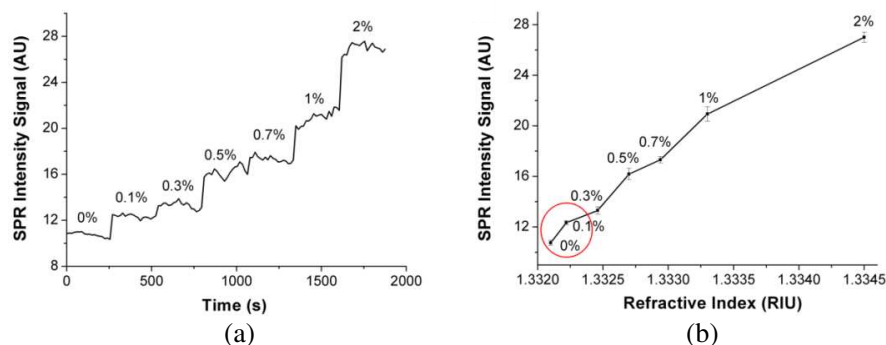
$$S_i = \frac{\Delta I_p}{\Delta n} = 1.328 \times 10^5 \, \text{A.U./RIU}$$

The standard deviation of the SPR intensity signal of 0.1% glycerine solution is regarded as the sensing uncertainty of the intensity interrogation method,

$$\sigma_i = 0.1646 \, \text{A.U.}$$

Finally we can calculate the resolution of the intensity interrogation method,

$$R_i = \frac{\sigma_i}{S_i} = 1.24 \times 10^{-5} \, \text{RIU}$$

Figure 7. (a) Intensity signal of p-polarization light when the probe channel is injected with different glycerine solutions. (b) The mean values and the standard deviations of the SPR intensity signal with different refractive index solutions.

Experimental result of our SPR-PI sensor shows that the resolution based on phase interrogation is 16 times higher than that based on intensity interrogation. The better resolution of the phase interrogation is mainly due to the larger dependence of the SPR phase shift on the sample refractive index change than the SPR intensity change. Moreover, the SPR phase signal is less sensitive to laser intensity noise than SPR intensity signal, which results into a lower standard deviation and consequently a higher resolution.

4.4. Protein Interaction Application

The gold spots of two selected vertical channels were self-assembled with Angiogenin before carrying out the detection of anti-Angiogenin. A DDA ethanol solution (5 mM) was injected into the two channels at a flow speed of 0.5 mL/h for 2 hours. The DDA molecules were adhered onto the gold film through the gold-thiol bond. Thereafter, the groups of -COOH of DDA molecules were activated by a mixed solution of EDC and NHS (both 12.5 mM) for 2 h. Then the channels were injected with a 0.1 mg/mL Angiogenin PBS solution at 0.1 mL/h to form a self-assembled layer on the gold surface. After 1 h, a PBS solution of BSA (10 mg/mL) was injected into the probe chamber to block the residual activated-COOH groups.

After Angiogenin functionalization, the vertical valves were opened and the horizontal valves were closed to allow samples flow horizontally. Six anti-Angiogenin solutions with different concentrations of 3.12, 6.25, 12.5, 50 and 100 µg/mL were injected into the 1–6 horizontal channels separately (0.15 mL/h), as indicated in Fig. 8(a). PBS solution was injected into the eighth channel as the reference. For each concentration solution, the SPR signals of the two reaction channels was calculated and averaged. The conjugation of anti-Angiogenin and angiogenin will increase the effective refractive index on the
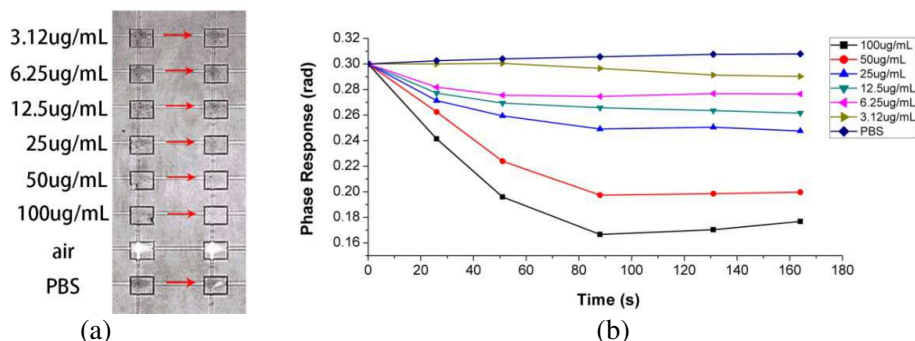
Figure 8. (a) CCD picture of the reaction chambers after the interaction between Angiogenin and anti-Angiogenin. Red arrows indicate the flow direction during the anti-Angiogenin injection. (b) Sensing diagram for the interaction between Angiogenin and anti-Angiogenin.

gold surface, so the SPR signal decreases after the injection of anti-Angiogenin solutions, as shown in Fig. 8(b). The SPR signal of the channel injected with the $100\,\mu g/mL$ solution decreases fastest. It indicates that more anti-body are captured and combined to the gold film with the $100\,\mu g/mL$ anti-Angiogenin solution. After 2 minutes interaction, the SPR signals of all concentrations solutions reach equilibriums. Anti-Angiogenin solutions with different concentrations can be clearly distinguished by their SPR phase signals after reach the equilibriums.

5. CONCLUSION

We propose a novel prism phase modulator (PPM) to modulate the phase difference between p- and s-polarization lights and apply it in a SPR-PI sensor. A homemade microfluidic device is applied to realize parallel detection. Experiment results of glycerine solution show that the resolutions of the SPR-PI sensor based on phase interrogation and intensity interrogation are about 7.61×10^{-7} RIU and 1.24×10^{-5} RIU, respectively. Immunoassay of the Angiogenin and anti-Angiogenin interaction has also been demonstrated. The most important features of the PPM are its great thermal reliability, ease of use, and low cost compared with other reported modulators. Since the PPM does not change the light path during modulation, its performance is steady to system vibration. Therefore, this work demonstrates a promising performance of PPM and great potential in practical applications.

REFERENCES

1. Homola, J., "Surface plasmon resonance sensors for detection of chemical and biological species," *Chemical Reviews*, Vol. 109, No. 2, 462–493, 2008.
2. Liedberg, B., C. Nylander, and I. Lundstrom, "Surface plasmon resonance for gas detection and biosensing," *Sensors and Actuators*, Vol. 4, No. 2, 299–304, 1983.
3. Ouellet, E., C. Lausted, T. Lin, C. W. T. Yang, L. Hood, and E. T. Lagally, "Parallel microfluidic surface plasmon resonance imaging arrays," *Lab on a Chip*, Vol. 10, No. 5, 581–588, 2010.
4. Luo, Y. Q., F. Yu, and R. N. Zare, "Microfluidic device for immunoassays based on surface plasmon resonance imaging," *Lab on a Chip*, Vol. 8, No. 5, 694–700, 2008.
5. Schasfoort, R. B. M. and A. J. Tudos, *Handbook of Surface Plasmon Resonance*, Royal Society of Chemistry, London, 2008.
6. Piliarik, M. and J. Homola, "Surface plasmon resonance (SPR) sensors: Approaching their limits?" *Optics Express*, Vol. 17, No. 19, 2009.
7. Kruchinin, A. A. and Y. G. Vlasov, "Surface plasmon resonance monitoring by means of polarization measurement in reflected light as the basis of DNA-probe biosensor," *Sensors and Actuators B*, Vol. 30, No. 1, 77–78, 1996.
8. Nelson, S. G., K. S. Johnston, and S. S. Yee, "High sensitivity surface plasmon resonance sensor based on phase detection," *Sensors and Actuators B*, Vol. 35, Nos. 1–3, 187–191, 1996.
9. Kabashin, A. V. and P. I. Nikitin, "Surface plasmon resonance interferometer for bio- and chemical-sensors," *Optics Communications*, Vol. 150, Nos. 1–6, 5–8, 1998.
10. Li, Y. C., Y. F. Chang, L. C. Su, and C. Chou, "Differential-phase surface plasmon resonance biosensor," *Analytical Chemistry*, Vol. 80, No. 14, 5590–5595, 2008.

11. Markowicz, P. P., W. C. Law, A. Baev, P. N. Prasad, S. Patskovsky and A. V. Kabashin, "Phase sensitive time-modulated surface plasmon resonance polarimetry for wide dynamic range biosensing," *Optical Express*, Vol. 15, No. 4, 1745–1754, 2007.

12. Huang, Y. H., H. P. Ho, S. Y. Wu, S. K. Kong, W. W. Wong, and P. Shum, "Phase sensitive SPR sensor for wide dynamic range detection," *Optics Letters*, Vol. 36, No. 20, 4092–4094, 2011.

13. Wang, R., C. L. Zhang, Y. Yang, S. W. Zhu, and X.-C. Yuan, "Focused cylindrical vector beam assisted microscopic pSPR biosensor with an ultra wide dynamic range," *Optics Letters*, Vol. 36, No. 11, 2091–2093, 2012.

14. Shao, Y. H., Y. Li, D. Y. Gu, K. Zhang, J. Qu, J. He, X. J. Li, S. Y. Wu, H. P. Ho, M. G. Somekh, and H. B. Niu, "Wavelength-multiplexing phase-sensitive surface plasmon imaging sensor," *Optics Letters*, Vol. 38, No. 9, 1370–1372, 2013.

15. Grigorenko, A. N., P. I. Nikitin, and A. V. Kabashin, "Phase jumps and interferometric surface plasmon resonance imaging," *Applied Physics Letters*, Vol. 75, No. 25, 3917–3919, 1999.

16. Notcovich, A. G., V. Zhuk, and S. G. Lipson, "Surface plasmon resonance phase imaging," *Applied Physics Letters*, Vol. 76, No. 13, 1665–1667, 2000.

17. Piliarik, M., H. Vaisocherova, and J. Homola, "A new surface plasmon resonance sensor for high-throughput screening applications," *Biosensors and Bioelectronics*, Vol. 20, No. 10, 2104–2110, 2005.

18. Wong, C. L., H. P. Ho, Y. K. Suen, S. K. Kong, Q. L. Chen, W. Yuan, and S. Y. Wu, "Real-time protein biosensor array based on surface plasmon resonance differential phase imaging," *Biosensors and Bioelectronics*, Vol. 24, No. 4, 606–612, 2008.

19. Piliarik, M., L. Parova, and J. Homola, "High-throughput SPR sensor for food safety," *Biosensors and Bioelectronics*, Vol. 24, No. 5, 1399–1404, 2009.

20. Huang, Y. H., H. P. Ho, S. K. Kong, and A. V. Kabashin, "Phase-sensitive surface plasmon resonance biosensors: Methodology, instrumentation and applications," *Annalen der Physik*, Vol. 524, No. 11, 637–662, 2012.

21. Hooper, I. R. and J. R. Samble, "Sensing using differential surface plasmon resonance ellipsometry," *Journal of Applied Physics*, Vol. 96, No. 5, 3004–3011, 2004.

22. Hopper, I. R. and J. R. Sambles, "Differential ellipsometric surface plasmon resonance sensor with liquid crystal polarization modulators," *Applied Physics Letters*, Vol. 85, No. 15, 3017–3019, 2004.

23. Wu, S. Y., H. P. Ho, W. C. Law, and C. Lin, "Highly sensitive differential phase-sensitive surface plasmon resonance biosensor based on the Mach-Zehnder configuration," *Optics Letters*, Vol. 29, No. 20, 2378–2380, 2004.

24. Su, Y. D. and S. J. Chen, "Common-path phase-shift interferometry surface plasmon resonance imaging system," *Optics Letters*, Vol. 30, No. 12, 1488–1490, 2005.

25. Ho, H. P., W. C. Law, S. Y. Wu, X. H. Liu, S. P. Wong, C. Lin, and S. K. Kong, "Phase-sensitive surface plasmon resonance biosensor using the photoelastic modulation technique," *Sensors and Actuators B*, Vol. 114, No. 1, 80–84, 2006.

26. Patskovsky, S., R. Jacquemart, M. Meunier, G. D. Crescenzo, and A. V. Kabashin, "Phase-sensitive spatially-modulated surface plasmon resonance polarimetry for detection of biomolecular interactions," *Sensors and Actuators B*, Vol. 113, No. 2, 628–631, 2008.

27. Kretschmann, E. and H. Z. Raether, "Radiative decay of non radiative surface plasmons excited by light (Surface plasma waves excitation by light and decay into photons applied to nonradiative modes)," *Zeitschrift Fuer Naturforschung, Teil A*, Vol. 23, 2135, 1968.